Proc. Natl. Acad. Sci. USA
Vol. 84, pp. 4984–4988, July 1987
Immunology

Construction of an extended three-dimensional idiotope map by electron microscopic analysis of idiotope–anti-idiotope complexes

(antibody/immunoglobulin/idiotype/epitope/immune complex)

KENNETH H. ROUX*, WILLIAM J. MONAFO†, JOSEPH M. DAVIE†, AND NEIL S. GREENSPAN†‡

*Department of Biological Science, Florida State University, Tallahassee, FL 32306; and †Departments of Microbiology and Immunology and Pathology, Washington University School of Medicine, St. Louis, MO 63110

Communicated by J. Herbert Taylor, March 23, 1987 (received for review January 21, 1987)

ABSTRACT **A three-dimensional map of the positions of four idiotypic determinants (idiotopes or Ids) and an isotypic determinant was derived by transmission electron microscopy of negatively stained immune complexes. Each complex was composed of a monoclonal Id-expressing IgG and one or two varieties of monoclonal anti-Id (or anti-isotype) Fab fragment or IgG. Data from the various combinations of Id and anti-Id (and anti-isotype) were used to construct a low-resolution three-dimensional model that revealed not only the approximate locations of Ids on the surface of the antibody variable domains but also details of the geometry of Id–anti-Id interactions not otherwise available. The Ids were shown to be dispersed over the variable domains, extending from the complementarity-determining region to near the variable–constant switch region. Thus, immunoelectron microscopy is a useful complement to serologic, biochemical, and genetic strategies for the topographical analysis of immunoglobulin Ids or other epitopes. This same approach should be of broader applicability in the study of epitopes and receptor sites on other macromolecules.**

A fundamental property of antibodies (Abs) is the ability to bind other molecules, including not only foreign antigens (Ags), but also self Ags, such as other immunoglobulins. The observation that Abs can be raised against the clone-specific portion (idiotope or Id) of the immunoglobulin variable domain (V) that confers Ag-binding specificity to the Ab (1, 2) has been of enormous practical significance for the study of the genetics (3) and clonal dynamics (4–7) of humoral immune responses. In addition, the discovery of idiotypy was a necessary precursor to the formulation of the network hypothesis of immune regulation (8), a concept that has had a major impact on experimental approaches in immunology and medicine. While these and subsequent developments have established the importance of Ids in understanding many aspects of immunity, the structural basis for idiotypy and its contribution to immune regulation and pathogenesis remains only partially understood.

Ab reactions with many immunoglobulin Ids are hapten inhibitable and thus the Ids are presumed to be at or near the distal tip of the Fab arms—i.e., in or adjacent to the complementarity-determining region (CDR). This is consistent with the observation that Id-specific amino acid substitutions tend to be clustered in the hypervariable regions (9–12) and, as such, derive from the same diversity-generating mechanisms that lead to Ag-binding diversity (13, 14). Examples of Id–anti-Id reactions that are not hapten inhibitable have also been reported (15).

The various techniques used to map immunoglobulin Ids often give fragmentary clues to their topographical location. Traditional serological approaches have the advantage of being broadly applicable (16–19). Disadvantages relate to possible artifacts associated with adsorbing one component of a system to a solid phase (20, 21). Also, mutually inhibitory Abs are often tacitly assumed to recognize adjacent or overlapping contact points and, if hapten inhibits an Id–anti-Id reaction, the Id is presumed to be in or adjacent to the CDR. These assumptions ignore the possibility that the reaction of Ab with an Id may conformationally alter a structure on a distant part of the molecule such that a second Id is created, modified, or lost (22, 23).

Efforts to localize Ids by using biochemically purified and isolated chains, domains, fragments, or synthetic peptides (24–26) are often unsuccessful because of the loss of conformation after chain separation or fragmentation. Amino acid sequence correlates (generally one to a few amino acid residues) critical to the expression of various Ids have been defined in several systems by comparing heavy and light chain V domain amino acid sequences from related myeloma and hybridoma proteins (27–29), or Id-loss variants (30–33). Unfortunately, these approaches do not unambiguously distinguish those amino acids that physically contribute to the Id from those for which amino acid substitutions yield (potentially distant) conformational adjustments that influence the expression of the Id (22, 23). Also, if one can extrapolate from the recently solved x-ray crystallographic structure of the complex between lysozyme and an anti-lysozyme monoclonal antibody (mAb) Fab fragment (34), an Id will probably involve many more amino acids than have been identified through these genetic analyses to date.

In this report we describe the application of immunoelectron microscopy (IEM) to the problem of determining spatial relationships of Ids and the geometry of Id–anti-Id interactions. IEM was used 20 years ago to show the general outline of the IgG molecule and to document bivalency and the location of the CDR (35). The increased resolution of modern electron microscopes has facilitated studies designed to discriminate between immunoglobulin allotopes and Ids on the basis of topographical location (36, 37), determine the degree of rotational flexibility of the hinge region (37, 38), and document the change in conformation of the Fc region after partial reduction (39). In the present study we demonstrated that a careful analysis of the fine structure of immune complexes composed of Id and anti-Id Ab can be used to construct a truly three-dimensional Id map and provide direct evidence that Ids may be located at points distant from the CDR. Moreover, not only are the approximate locations of

The publication costs of this article were defrayed in part by page charge payment. This article must therefore be hereby marked "*advertisement*" in accordance with 18 U.S.C. §1734 solely to indicate this fact.

Abbreviations: Id, idiotope; IdI, individual idiotope; IdX, crossreactive idiotope; Ab, antibody; mAb, monoclonal Ab; Ag, antigen; Fab, Ag-binding fragment or region of Ab; Fv, variable regions of Fab; CDR, complementarity-determining region; V, variable region of immunoglobulin; C_κ, constant region of the κ light chain; H chain, heavy chain; L chain, light chain; IEM, immunoelectron microscopy; GAC, streptococcal group A carbohydrate.

‡Present address: Institute of Pathology, Case Western Reserve University, Cleveland, OH 44106.

the Ids revealed but also their orientations and the geometries of the Id-anti-Id complexes are suggested.

MATERIALS AND METHODS

mAb and Fab Fragment Production and Characterization. The generation and maintenance of somatic cell hybrids secreting HGAC 39 and anti-idiotype antibodies specific for HGAC 39 and the purification of these antibodies have been described (16, 40). The hybridoma 187.1, secreting anti-mouse κ-chain constant region (C_κ) mAb, was originally obtained from the laboratory of M. D. Scharff (41). Anti-Id Fab fragments were produced by digestion of affinity-purified or ammonium sulfate-precipitated anti-Id with papain (Cooper Biomedical, Malvern, PA) (42); the fragments were judged to be free of whole-molecule contamination by sodium dodecyl sulfate/polyacrylamide gel electrophoresis.

IEM. IgG, Fab, and immune complexes were prepared and negatively stained as previously described (36, 39). Freshly cleaved mica sheets (4 by 10 mm) were coated with a thin carbon film. The films were successively floated onto a 1% tryptophan solution (10 sec), water (15 sec), IgG, Fab, or immune complex at 2–10 μg/ml in 0.15 M ammonium acetate (10 sec), 0.3 M ammonium acetate (15 sec), and a 2% uranyl formate staining solution (60 sec). The reagents were placed as large droplets onto a Teflon ring slide and maintained at 4°C. A 600-mesh copper grid (Polyscience, Warrington, PA) (polished side down) was gently placed upon the carbon film floating on the stain. The copper grid with the adherent carbon membrane was rapidly removed from the surface of the stain well. Excess stain was then removed by capillary action. This procedure causes the carbon membrane to fold over on itself, trapping a thin film of stain between two immunoglobulin-coated layers. The grids were examined on a JEOL JEM CX-100 electron microscope and photographed at 100,000 diameters magnification. Negatives were printed at ×260,000 for analysis.

RESULTS

Visualization of Id–Anti-Id Fab Complexes. We chose to study the Id–anti-Id system defined by the murine mAb HGAC 39 (40), an A/J IgG3κ Ab specific for streptococcal group A carbohydrate (GAC), and four rat mAb anti-Ids elicited by HGAC 39. In previous studies (16) solid-phase competitive binding assays, in which anti-Ids competed with hapten or with one another for binding to HGAC 39, were employed to operationally map the Ids recognized by the rat anti-Ids. This map was of particular interest because it appeared to define four sequentially overlapping Ids extending from near the CDR (the distal end of the V domain) to a site close to the switch junction between the V and constant (C) domains (i.e., the proximal end of the V domain).

For the present study, mapping by IEM was initially carried out by visualizing HGAC 39 in complex with one or another of each of the anti-Id mAb Fabs as well as anti-C_κ Fab. To deduce the location of the various Ids, several parameters of each complex were measured as illustrated in Fig. 1. First, the immune complexes were scored for the angle at which the Fab Ab bound to the Fab arm of HGAC 39 (Fig. 1*A*). Second, the relative proximal–distal site of interaction with respect to the tip of the Fab arm of HGAC 39 was determined—i.e., whether the Fab Ab binds near the tip, near the V–C junction, or at an intermediate position (Fig. 1*B*). These procedures have previously been used to discriminate between distally binding anti-Id Ab and more proximally binding anti-V_H Ab on rabbit and mouse IgG molecules (36, 43, 44). In the present study we have further refined our analysis by scoring each complex for the rotational orientations of both the Fab Ab and the Fab arm of HGAC 39 with respect to the plane of the carbon support membrane. For this comparison the general outline of the Fab molecules or arms

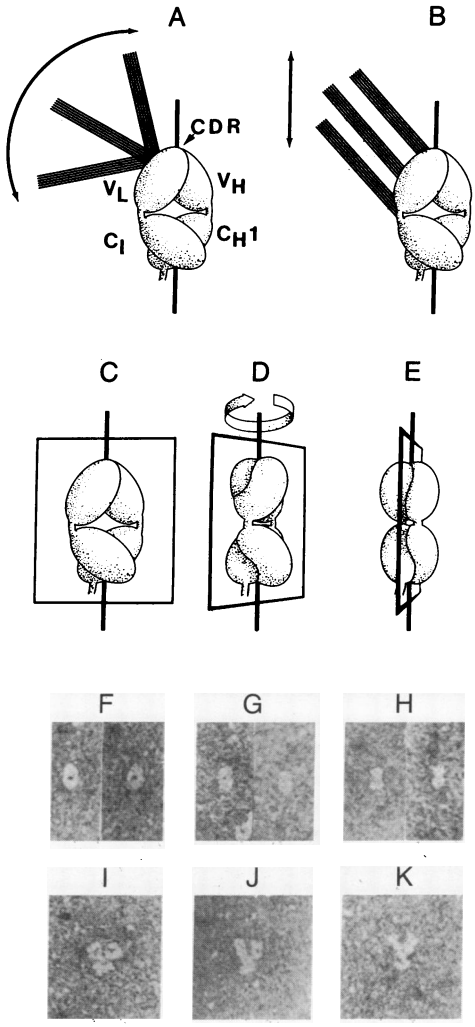

FIG. 1. Depiction of three of the parameters scored for each Fab of an immune complex. CDR, heavy (H) chain (V_H and C_H), and light (L) chain (V_L and C_L) components of Fab are delineated for ease of interpretation but are not distinguishable in the electron micrographs. (*A*) Angle at which the Ab probe (represented by parallel lines) and target Ab intersect with reference to their proximal–distal axes. (*B*) Relative proximal–distal intersect. (*C–E*) Rotational plane of the target or probe Fab. Each Fab component was judged to be either planar (*C*), intermediate (*D*), or perpendicular (*E*) with respect to the carbon membrane. (*F*, *G*, and *H*) Electron micrographs of representative free Fabs corresponding to the planar, intermediate, and perpendicular configurations, respectively. (*I*, *J*, and *K*) Electron micrographs of intact IgG with Fab (upward-extending arms) in the planar configuration (*I*), intermediate configuration (right arms of *J* and *K*), and perpendicular configuration (left arms of *J* and *K*). (*F–K*, ×330,000.)

was compared to published computer-generated models of Fab derived from x-ray diffraction data (45). Our interpretations were facilitated by the distinctive profiles of Fab at various orientations about its long axis. When the plane of Fab (defined as a plane transecting its widest aspect and passing through its proximal–distal axis of rotation) is parallel to the plane of the carbon membrane, Fab appears slightly oblong with a central stain-filled cavity (Fig. 1*C*). Viewed "on edge" (i.e., rotated 90° about its proximal–distal axis), Fab appears as a bilobed structure (Fig. 1*E*). An intermediate degree of rotation yields an elongate oval either with or without a less prominent central opening and an occasional medial constriction (Fig. 1*D*). Examples of electron micrographs of Fab showing these various configurations are shown in Fig. 1 *F*, *G*, and *H*, respectively. Fig. 1 *I*, *J*, and *K*

shows intact IgG molecules exhibiting Fab arms in each of the three rotational orientations.

The data described below were obtained from the analysis of between 50 and 250 immune complexes of each type and were used in constructing a three-dimensional Id–anti-Id model. The locations and orientations of the various anti-Id and anti-isotype components of the model were adjusted such that the greatest number of images of each type could be reconciled with the model. The five mAbs formed clearly identifiable complexes with HGAC 39 as shown in Fig. 2. Fab anti-IdI-2 was found to react with the most distal idiotope identified. Even so, the anti-IdI-2 binds slightly lateral to the distal tip and projects about 20° from the proximal–distal axis of the target Fab arm of HGAC 39. The Fab Ab and the target Fab are in the same planar orientation. Fab anti-IdI-3a, -IdI-1, and -IdX Abs bind at progressively more proximal sites (lateral to distal tip, ⅓ distal from the switch region, and ¼ distal from the switch region, respectively) and project at progressively greater angles (approximately 40°, 60°, and 100°, respectively). Thus the Ids recognized by these Abs are not clustered about the CDR but are scattered over the surface of the Fv region (the V regions of Fab). Fab anti-IdX, in fact, appears to bind just distal to the V–C switch region. The anti-isotypic Fab Ab, anti-C_κ (competitive with anti-IdX) (16), binds ¼ proximal to the V–C switch region at an angle of about 110°. With the exception of anti-IdI-2 as noted above, each of the Fab Abs binds to HGAC 39 such that the planes of the reactants are more or less perpendicular to one another.

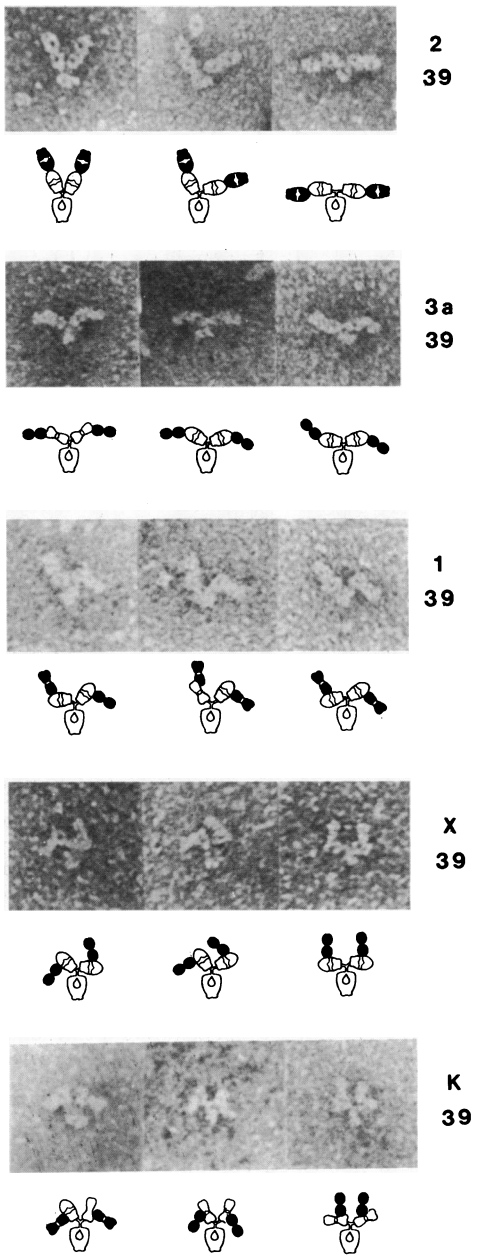

FIG. 2. Electron micrographs (above; ×350,000) and interpretive diagrams (below) of HGAC 39 in complex with anti-Id mAb Fab. HGAC 39 is represented in the diagrams as an open figure and the Fab Ab probes are represented as solid figures. The Fab arms of the Ab targets and probes are drawn to indicate their rotational orientation as planar (oval with open center), intermediate ("bone shaped" with or without central opening), or perpendicular ("dumbbell shaped"). Abbreviations: 39, HGAC 39; 2, anti-IdI-2 Fab probe; 3a, anti-IdI-3a Fab probe; 1, anti-IdI-1 Fab probe; X, anti-IdX Fab probe; K, anti-C_κ Fab probe. Id designates an individual idiotype, and IdX, a crossreactive idiotype.

Analysis of Complexes Containing Id, Anti-Id Fab, and a Second, Noncompeting, Anti-Id IgG (Heterocomplexes). The analysis of complexes of Id IgG and anti-Id Fab (Fig. 2) served to localize the site of anti-Id binding to a given latitudinal band (i.e., the distance from the distal tip or the V–C switch region) on a target Fab arm of HGAC 39. However, because of the considerable rotational flexibility of the hinge region (≥180°) observed in IEM preparations (37, 38) and the approximate bilateral symmetry of the Fab, one of two general longitudinal sites of interaction (180° apart) is

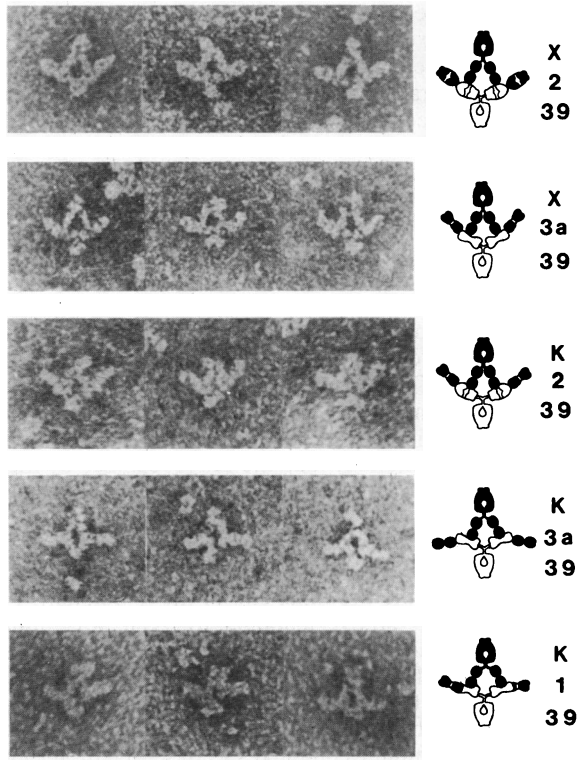

FIG. 3. Electron micrographs (*Left*; ×350,000) and composite interpretive diagrams (*Right*) of heterocomplexes composed of HGAC 39 (39), with IgG anti-IdX (X) or anti-C_κ (K), and Fab anti-IdI-2 (2), anti-IdI-3a (3a), or anti-IdI-1 (1). The complexes are oriented such that the IgG Ab probe is on top, HGAC 39 is on the bottom, and the Fab Ab probes project laterally. Diagram symbols are as described for Fig. 2. Some of the IgG components of the complexes appear distorted (i.e., HGAC 39 when complexed with anti-C_κ) as a result of a three-dimensional projection of some of the elements above (or downward toward) the surface of the carbon membrane. Thus, for example, the anti-IdI-1 Fab probes are interpreted (on the basis of the data in Fig. 2 and unreported complexes of HGAC 39 and intact anti-IdI-1) to be projecting diagonally above or below the Fab arms of HGAC 39 (bottom row; also see model in Fig. 4*C*).

possible. A discrimination between such alternatives was facilitated by the analysis of heterocomplexes in which HGAC 39 was allowed to react with two different mAbs (one intact IgG and the other as an Fab) simultaneously (Fig. 3). By comparing the geometries of the resulting complexes to those observed when each probe was used alone, a judgment could be made as to whether any given pair of probes bound to HGAC 39 on the same side, opposite sides, or at relatively intermediate positions with respect to one another.

Intact anti-IdX forms an easily interpretable complex with HGAC 39, reacting in the plane perpendicular to the plane of HGAC 39 Fab (data not shown). The intersect is just distal to the V–C switch region, a configuration consistent with complexes composed of Fab anti-IdX and HGAC 39 as shown in Fig. 2. Heterocomplexes with anti-IdX as the reference probe show that both anti-IdI-3a and anti-IdI-2 bind on the same side of HGAC 39 Fab as does anti-IdX (Fig. 3). In contrast to anti-IdX, intact anti-C_κ reacts with HGAC 39 to yield somewhat distorted configurations (data not shown). It seems likely that the interaction of the two arms of each of the reactants causes geometric constraints that do not allow the two molecules to lie in the same plane. Thus one or both molecules are projecting somewhat above the plane of the membrane, leading to perceptually foreshortened dimensions. In heterocomplexes, anti-IdI-3a binds opposite and anti-IdI-2 and -1 each bind intermediate with respect to the binding site of intact anti-C_κ (Fig. 3). Reciprocal heterocomplexes composed of Fab anti-IdX or anti-C_κ and intact anti-IdI-1, -2, or -3a in complex with HGAC 39 revealed geometries consistent with the above interpretations (data not shown).

With these data, the relative location of each Id with respect to each of the other Ids could be deduced to yield a three-dimensional topographical map (Fig. 4). Yet, because of the approximate bilateral symmetry of the Fab molecule, the resulting map could be superimposed upon either the L chain or the H chain. A discrimination between the alternatives was obvious in the case of HGAC 39, since previous serological and genetic analyses identified those determinants recognized by anti-C_κ, anti-IdX, and anti-IdI-1 as being expressed on the isolated L chain (16, 46–48). However, such information with regard to any one laterally located Id in such a map should be enough to assign a final orientation to an entire map. The placement of IdI-3a in the H chain was suggested by IEM analysis alone but has subsequently been supported by molecular genetic studies (48).

DISCUSSION

In the present report we demonstrate that IEM of two- and three-component Ag–Ab complexes can be used to determine topographic relationships of multiple epitopes (in this case Ids) expressed by a single pair of protein domains (Fv) of approximately 25 kDa.

Taken together, the IEM data allowed us to construct a true three-dimensional Id map based on direct evidence (Fig. 4). One of our primary goals was to determine whether operational Id maps derived exclusively from serological analyses accurately reflect the actual topographical location of the Ids. Several similarities as well as differences between the IEM-derived and serologically derived maps were apparent. As predicted (16), the Ids do appear to form a more or less continuous linear array, albeit rather sinuous, stretching from near the CDR to the V–C junction. Serological and IEM analyses both placed IdI-2 and IdI-3a distally, and IdI-1 and IdX progressively more proximally. Clearly, this direct evidence demonstrates that immunoglobulin Ids are not restricted to the area in or immediately adjacent to the CDR as generally perceived. It follows that some Ids may thus be dependent exclusively upon framework region contact residues rather than upon hypervariable residues. These findings support the predictions derived from hydrophilicity variability plots (49) that there should be several framework region idiotypic "hotspots." They are also consistent with recent studies demonstrating that substitution of the CDR regions from a donor V domain for the CDR regions of an unrelated recipient V domain yields a molecule that carries donor hapten specificity yet fails to express donor Ids (50).

A significant difference between the serologically derived and IEM-derived maps relates to the exact placement of IdI-2 and IdI-3a. Anti-IdI-2 and anti-IdI-3a are comparably inhibited from binding to HGAC 39 by either *N*-acetylglucosamine or GAC (16). Thus both of the corresponding Ids were assumed to be near the hapten binding site at the distal end of HGAC 39 V domain. Because anti-IdI-2 exhibited very weak inhibition of the binding of anti-IdX to HGAC 39, while anti-IdI-3a did not, it was hypothesized that anti-IdI-2 extended more proximally than IdI-3a (16). In contrast, the results of the IEM studies reported here indicate that IdI-2 is more distal than IdI-3a, although these two Ids probably overlap in the dimension defined by the proximal–distal axis.

An anti-Id bound to its Id may block access to an area larger than the Id (contact region) itself. This consideration is

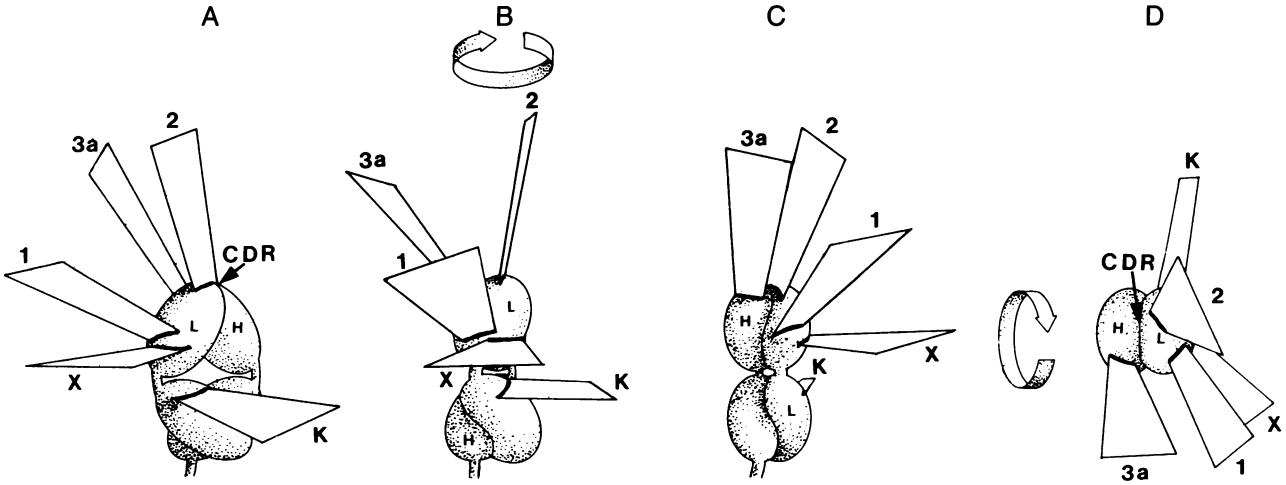

FIG. 4. Three-dimensional model of HGAC 39 Fab (stippled figures), depicting approximate Id locations and planes of Id–anti-Id intersect. The CDR is indicated for orientation. *A*, *B*, and *C* represent the rotation of HGAC 39 Fab through 90° on the proximal–distal axis from planar (*A*) to intermediate (*B*) and perpendicular (*C*). *D* represents a 90° rotation of *C* to allow a "top" view of the CDR. The projections from the surface of HGAC 39 represent three-dimensional depictions of rectangles corresponding to the planes (as defined in the text) of the various Fab Ab probes. The thickened bases of the rectangles represent the location and orientation of the Ids and the C_κ isotypic determinant. The diagrammatic details are not intended to suggest the size or degree of overlap of the Ids in this model. Abbreviations are as in Fig. 2.

of interest in trying to account for the mutually inhibitory effects of anti-Idl-2 and anti-Idl-1 (16), which appear to bind to topographically distant sites on the HGAC 39 Fv region (Figs. 2 and 4). Although a more detailed modeling of these interactions might reveal the spatial overlap of the bound anti-Ids, even if the Ids proper fail to overlap in space, these two anti-Ids might reciprocally induce conformational alterations and concomitant loss of Ids on the HGAC 39 Fv domain upon binding. In this context, the ability of the antigen GAC (about 10 kDa) to block binding of mAb to the proximally located Idl-1 on HGAC 39 is also of interest.

IEM as a tool for the study of the structural basis for Id–anti-Id interaction provides an important complement to serologic, genetic, and biophysical techniques. Although the resolution of electron microscopy is low in comparison to the data generated by crystallography, and only approximate interaction sites can be deduced, virtually any small Id–anti-Id complex can be readily visualized. Thus, the lack of precise resolution is, in part, offset by the considerable versatility and simplicity of the technique. Moreover, no crystallographic data on Id–anti-Id interactions have as yet been published.

IEM not only facilitates the construction of a truly three-dimensional Id map, it also reveals data extending beyond the surface of the target molecule. Specifically, the angles and rotational orientation of the anti-Id Ab as it interacts with the Id-bearing immunoglobulin may be deduced (Fig. 4). These variations in the geometry of the Id–anti-Id intersect may significantly influence the ultimate size and configuration, and thus the biological function, of the resulting complex (51–53). This type of information, which cannot be readily extracted by using the other approaches, should allow the testing of more elaborate models to give clues to the relationship between Id location and the quaternary structure of physiologically relevant immune complexes.

We thank Ms. S. Chapman for her skilled photographic assistance and Ms. L. Mathews for her help in the preparation of this manuscript. This work was supported by U.S. Public Health Service Grants AI 16596 (K.H.R.), AI 15926, and AI 15353. W.J.M. was supported by a Medical Student Research Fellowship from the American Heart Association.

1. Kunkel, H. G., Mannik, M. & Williams, R. C. (1963) *Science* **140,** 1218–1219.
2. Oudin, J. & Michel, M. (1963) *C.R. Acad. Sci. Ser. 3* **257,** 805–808.
3. Eichmann, K. (1975) *Immunogenetics* **2,** 491–506.
4. Hansburg, D., Briles, D. E. & Davie, J. M. (1976) *J. Immunol.* **117,** 569–575.
5. Hansburg, D., Briles, D. E. & Davie, J. M. (1977) *J. Immunol.* **119,** 1406–1412.
6. Briles, D. E. & Davie, J. M. (1980) *J. Exp. Med.* **152,** 151–160.
7. Cerny, J., Wallich, R. & Hammerling, G. J. (1982) *J. Immunol.* **128,** 1885–1891.
8. Jerne, N. K. (1974) *Ann. Immunol. (Paris)* **125C,** 373–389.
9. Kim, S., Davis, M., Sinn, E., Pattern, P. & Hood, L. (1981) *Cell* **27,** 573–581.
10. Kaartinen, M., Griffiths, G. M., Markham, A. F. & Milstein, C. (1983) *Nature (London)* **304,** 320–324.
11. McKean, D., Huppi, K., Bell, M., Staudt, L. & Gerhard, W. (1984) *Proc. Natl. Acad. Sci. USA* **81,** 3180–3184.
12. Cleary, M. L., Meeker, T. C., Levy, S., Lee, E., Trela, M., Sklar, J. & Levy, R. (1986) *Cell* **44,** 97–106.
13. Tonegawa, S. (1983) *Nature (London)* **302,** 575–581.
14. Teillaud, J.-L., Desaymard, C., Giusti, A. M., Haseltine, B., Pollock, R. R., Yelton, D. E., Zack, D. J. & Scharff, M. D. (1983) *Science* **222,** 721–726.
15. Kelus, A. J. & Gell, P. G. H. (1968) *J. Exp. Med.* **127,** 215–234.
16. Greenspan, N. S. & Davie, J. M. (1985) *J. Immunol.* **134,** 1065–1072.
17. Zenke, G., Eichmann, K. & Emmrich, F. (1985) *J. Immunol.* **135,** 4066–4072.
18. Streicher, H. Z., Cuttitta, F., Buckenmeyer, G. K., Kawamura, H., Minna, J. & Berzofsky, J. A. (1986) *J. Immunol.* **136,** 1007–1014.
19. Campbell, M., Bieber, M., Levy, R. & Teng, N. N. H. (1986) *J. Immunol.* **136,** 2983–2988.
20. Stevens, F. J., Jwo, J., Carperos, W., Kohler, H. & Schiffer, M. (1986) *J. Immunol.* **137,** 1937–1944.
21. Soderquist, M. E. & Walton, A. G. (1980) *J. Colloid Interface Sci.* **75,** 386–397.
22. Furey, W., Jr., Wang, B. C., Yoo, C. S. & Sax, M. (1983) *J. Mol. Biol.* **167,** 661–692.
23. de la Paz, P., Sutton, B. J., Darsley, M. J. & Rees, A. R. (1986) *EMBO J.* **5,** 415–425.
24. McMillan, S., Seiden, M. V., Houghten, R. A., Clevinger, B., Davie, J. M. & Lerner, R. A. (1983) *Cell* **35,** 859–863.
25. Chen, P. P., Houghten, R. A., Fong, S., Rhodes, G. H., Gilbertson, T. A., Vaughan, J. H., Lerner, R. A. & Carson, D. A. (1984) *Proc. Natl. Acad. Sci. USA* **81,** 1784–1788.
26. Barlow, D. J., Edwards, M. J. & Thornton, J. M. (1986) *Nature (London)* **322,** 747–748.
27. Rudikoff, S. (1983) *Contemp. Top. Mol. Immunol.* **90,** 169–209.
28. Rajewsky, K. & Takemori, T. (1983) *Annu. Rev. Immunol.* **1,** 569–607.
29. Davie, J. M., Seiden, M. V., Greenspan, N. S., Lutz, C. T., Bartholow, T. L. & Clevinger, B. L. (1986) *Annu. Rev. Immunol.* **4,** 147–165.
30. Bruggemann, M., Radbruch, A. & Rajewsky, K. (1982) *EMBO J.* **1,** 629–634.
31. Radbruch, A., Zaiss, S., Kappen, C., Bruggemann, M., Beyreuther, K. & Rajewsky, K. (1985) *Nature (London)* **315,** 506–508.
32. Bruggemann, M., Muller, H.-J., Burger, C. & Rajewsky, K. (1986) *EMBO J.* **5,** 1561–1566.
33. Jeske, D., Milner, E. C. B., Leo, O., Moser, M., Marvel, J., Urbain, J. & Capra, J. D. (1986) *J. Immunol.* **136,** 2568–2574.
34. Amit, A. G., Mariuzza, R. A., Phillips, S. E. V. & Poljak, R. J. (1986) *Science* **233,** 747–753.
35. Valentine, R. C. & Green, N. M. (1967) *J. Mol. Biol.* **27,** 615–617.
36. Roux, K. H. & Metzger, D. W. (1982) *J. Immunol.* **129,** 2548–2553.
37. Roux, K. H. (1984) *Eur. J. Immunol.* **14,** 459–464.
38. Wrigley, N. G., Brown, E. B. & Skehel, J. J. (1983) *J. Mol. Biol.* **169,** 771–774.
39. Seegan, G. W., Smith, C. A. & Schumaker, V. N. (1979) *Proc. Natl. Acad. Sci. USA* **76,** 907–911.
40. Nahm, M. H., Clevinger, B. L. & Davie, J. M. (1982) *J. Immunol.* **129,** 1513–1518.
41. Yelton, D. E., Desaymard, C. & Scharff, M. D. (1981) *Hybridoma* **1,** 5–11.
42. Rousseaux, J., Rousseaux-Prevost, R. & Bazin, H. (1983) *J. Immunol. Methods* **64,** 141–146.
43. Roux, K. H., Metzger, D. W., Kazdin, D. S. & Horng, W. J. (1984) *Eur. J. Immunol.* **14,** 910–915.
44. Van Cleave, V. H., Murti, K. G. & Metzger, D. W. (1986) *Eur. J. Immunol.* **16,** 701–707.
45. Silverton, E. W., Navia, M. A. & Davies, D. R. (1977) *Proc. Natl. Acad. Sci. USA* **74,** 5140–5144.
46. Greenspan, N. S., Fulton, R. J. & Davie, J. M. (1986) *J. Immunol.* **137,** 228–233.
47. Greenspan, N. S. & Monafo, W. J. (1987) *Int. Rev. Immunol.* **2,** 389–415.
48. Lutz, C. T., Bartholow, T. L., Greenspan, N. S., Fulton, R. J., Monafo, W. J., Perlmutter, R. M., Huang, H. V. & Davie, J. M. (1987) *J. Exp. Med.* **165,** 531–545.
49. Kieber-Emmons, T. & Kohler, H. (1986) *Immunol. Rev.* **90,** 29–48.
50. Jones, P. T., Dear, P. H., Foote, J., Neuberger, M. S. & Winter, G. (1986) *Nature (London)* **321,** 522–525.
51. Mannick, M. (1980) *J. Invest. Dermatol.* **74,** 333–338.
52. Goldman, M., Renversez, J. C. & Lambert, P. H. (1983) *Springer Semin. Immunopathol.* **6,** 33–49.
53. Greenspan, N. S., Monafo, W. J. & Davie, J. M. (1987) *J. Immunol.* **138,** 285–292.